Evaluation of the air-borne ultrasound on fluidized bed drying of shelled corn: Effectiveness, grain quality and energy consumption

Journal:	*Drying Technology*
Manuscript ID	LDRT-2017-0235.R4
Manuscript Type:	General Paper
Date Submitted by the Author:	n/a
Complete List of Authors:	Abdoli, Baharh; Shiraz University, Biosystems Engineering Zare, Dariush; Shiraz University, Biosystems Engineering Jafari, Abdolabbas; Shiraz University Chen, Guangnan ; University of Southern Queensland, Faculty of Health, Engineering and Sciences
Keywords:	Quality attributes, Drying kinetics, Ultrasound-assisted fluidized bed dryer, Machine vision, Artificial neural network

For Peer Review Only

SCHOLARONE™
Manuscripts

Evaluation of the air-borne ultrasound on fluidized bed drying of shelled corn: Effectiveness, grain quality and energy consumption

Bahareh Abdoli[1], Dariush Zare[1*],AbdolabbasJafari[1,2], GuangnanChen[3]

[1] *Biosystems Engineering Department, Shiraz University, Shiraz, P.O.Box. 71441-6518, Iran*

[2]*Lincoln Agritech Ltd, Lincoln University, Lincoln 7640, New Zealand*

[3] *Faculty of Health, Engineering and Sciences, University of Southern Queensland, Toowoomba, QLD 4350, Australia*

Abstract

The objective of the study was to investigate the influence of high power ultrasound on a laboratory-scale fluidized bed shelled corn dryer. The drying time, moisture content variation, specific energy consumption and quality parameters including ultimate compressive strength, toughness, shrinkage and color of corn kernels were investigated. Furthermore, Artificial Neural Network (ANN) simulation models were developed for predicting the drying variables. Machine vision techniques were used to determine color and shrinkage as qualitative indices. Results showed that the lower frequencies had better penetrations at lower temperatures and cause a significant reduction in drying time. In addition, the ultrasound application led to reduction of ultimate compressive strength and toughness of the dried samples although ultrasound has non-thermal character as the subsidiary factor, it plays an important role in shrinkage and color specification. Based on error analysis results, the prediction capability of ANN model is found to be reasonable for the developed models. Application of ultrasound significantly decreased the specific energy consumption (SEC) of drying process at the optimal drying condition.

Keywords: Quality attributes, Drying kinetics, Ultrasound-assisted fluidized bed dryer, Machine vision, Artificial neural network

For Peer Review Only

*Corresponding Author:D. Zare, Associate Prof., Shiraz University, E-Mail:sanyzare@yahoo.com or bahareh.abdoli@yahoo.com, Tel.: +987116138192,Fax: +98-71-32286187.

1. Introduction

Corn (*Zea mays L*) is one of the most important cereal sources in the world, providing a source of high quality proteins for both feed and food applications [1]. Freshly harvested corn contains high level of moisture (32-43 %d.b, equivalent to24-30 %w.b) at which storability is impossible. Therefore moisture content should be reduced to the level of 16-17 %d.b (equivalent to13.8-14.5 %w.b) after harvest[2]. Fluidized bed drying is the most commonly used drying method to preserve foods and agricultural products[3,4,5]and among several methods for drying of moist granular materials, fluidized bed drying has been one of the most successful techniques and widely used during postharvest processing of agricultural grain. In this drying method, solid moist particles are suspended in a hot air stream and a high rate of heat and mass transfer take place between the grain and gas. These types of dryers consume a considerable amount of energy and suffer from long drying time and such methods may produce structural changes in the products [6,7,8]. Researchers are looking for new technologies of grain processing which introduce new secure drying methods for better quality of grains for local and export markets. Among new technologies beginning to develop and becoming famous, ultrasonic dehydration is very desirable because the effects of ultrasound are more significant at low temperature which consequently decreases the contingency of food degradation. Moreover, ultrasound is an appropriate for treatment of heat sensitive products without any inner-heat increase, therefore food quality can be preserved [9,10,11,12,13]. Compared with other drying techniques in fluidized bed drying, the entire bed is dried homogenously. However air-born ultrasound assisted fluidized bed drying is new technique of drying in which food stuffs is suspended in the air stream while ultrasound energy being introduced to the bed via an appropriate ultrasound transducer. The new proposed drying method of moist granular materials can help use the advantages of both drying methods [1314].Several investigators have been involved in development of an ultrasonic dehydration method and improving drying process based on indirect contact with the food products such as potato [10], paddy [13], vegetables [15], persimmon [16], button mushrooms, Brussels sprouts and cauliflower [17], banana [18], melon [19], sapota [20], soy [21], carrot and lemon peel [22], pineapple [23], strawberries [24], apple [25], red bell pepper [26], green pepper [27] and carrot [28].The results of some of the mentioned cases showed that ultrasound treatment reduced drying time significantly [29,30,31].

When the ultrasonic wave is applied to the material which to be dried, it passes through the solid medium creating rapid series of alternative compressions and expansions in a similar way to a sponge when it is squeezed and released repeatedly (sponge effect). In this mechanical mechanism, the involved forces can exceed surface tension force which keeps the moisture within the capillaries of the material, creating micro-channels which may make the moisture elimination easier. These micro-channels were first submitted in micrographs by Fernandes et al. [19]in melon tissue after using ultrasound. Furthermore, for removal of much moisture ultrasound produces cavitation this may help the phenomenon. Other efficacies caused by ultrasound to be considered are surface tension, the variation of viscosity, the deformation of the porous solid material [10,32,33] and another effect is responsible for the development of microscopic channels, diminishing the diffusion of boundary layer and augmenting the convective mass transfer in food material [10].

One of the methods for monitoring the product quality during drying procedure is image processing [34]. A rather new and precise method to determine physical characteristics of agricultural products is also application of machine vision. It can efficiently be used for determination of qualitative characteristics of the product where there is a strong correlation between those characteristics and visual features. Therefore, in such cases machine vision can be used in a dryer for real time monitoring of physical quality of the product. It may use an algorithm to determine surface area of some axisymmetric agricultural products including eggs, lemons, limes and peaches [35] and study the effect of drying

URL: http:/mc.manuscriptcentral.com/ldrt Email: mpeasm@nus.edu.sg

For Peer Review Only

process on shrinkage, color and some other visual features of the product being dried [36].In case of food industry some properties such as shape (shrinkage) and color are to be determinant for quality of the dried product.

Artificial Neural Network (ANN) is a computational approach recently used in simulation and prediction of some parameters in drying processes. ANNs overcome the restrictions of conventional computing approaches by extracting the required information from the input data. They do not need specific equations. However, they need to be feed by adequate amount of input and output data [37]. According to the literature, there is no published information on shelled corn drying in an ultrasound-assisted fluidized bed dryer. Therefore the major objectives of the present study are:

(1) Evaluation of drying kinetics of corn in an ultrasound-assisted fluidized bed dryer

(2) Quality assessment of dried corns in terms of ultimate compressive strength, toughness of grain kernels and employing image processing for analyzing shrinkage and color

(3) To develop and evaluate ANN models to predict the shelled corn drying characteristics and quality

(4) Verifying the optimum energy consumption of the dryer by considering product quality in order to contribute to further energy saving and preserving the quality during drying

2. Material and Methods

2.1. Preparation of samples

Fresh corn was prepared from a local farm near Shiraz, a south-western city of Iran. Shelled corn was cleaned to remove all foreign, broken and disinfected materials for preventing mold development. The grains were carefully selected so that the most uniform shaped ones were gathered. In order to avoid moisture loss, the samples were kept in separate polythene bags and stored in a refrigerator at 4±0.5^{o}C.

2.2. Ultrasound treatment

In this study an experimental ultrasound-assisted fluidized bed dryer developed by Jafari and Zare(2016) [13] were modified and employed for drying process of corn [14] (Fig. 1).

The airflow unit of the drying apparatus included a variable speed centrifugal fan controlled by an inverter (N50-007SF, Korea) and to obtain the desire inlet temperature, an electric heating unit containing 1kW as well as two 0.5 kW electric heater elements was supplied. The bed thickness was about 4cm and the minimum speed of airflow required for fluidization entering the bed was kept constant at 0.79±0.21 m/s during all the tests. Air speed was measured with Testo435-2 (Germany, ±0.03m/s) and the temperature and relative humidity of the drying air were measured using a Testo625(Germany, ±0.5^{o}C, ±2.5%RH).A temperature controller (SU-105IP, Samwon Engineering, Korea) was used to control the inlet temperature of the system at a fixed pre-defined value and it was equipped with a K-type thermocouple with an accuracy of ±1^{o}C.In order to create high intensity ultrasonic field inside the fluidized bed drying chamber and to avoid sound transmission loss, dryer chambers were made of the same material piezoelectric transducers, an aluminum cylinder (with internal diameter of 130 mm, height of 250mm and thickness of 10 mm) was prepared. Aluminum cylinder was milled at one side of peripheral surface so that the piezoelectric transducers could be placed and bolted tightly. Different piezoelectric transducers (PZT-8 20kHz100W, PZT-4 25kHz100W, PZT-4 28kHz100W, PZT-8 30kHz100W, China) were selected and an appropriate high power ultrasound generator (UCE Ultrasonic PCB, max power 300W, 230V, China) was employed to activate the transducers [13-14] (Fig. 2).

2.3. Drying procedure

For each experiment 326±10g of shelled corn with average initial moisture content of 31.5±0.5(kg/kg, %d.b) determined according to the standard oven drying method (i.e., heating at 103^{o}C for 72h) was filled into the drying bed.

URL: http:/mc.manuscriptcentral.com/ldrt Email: mpeasm@nus.edu.sg

For Peer Review Only

The drying operation continued until the final moisture content of 16±0.5(kg/kg, %d.b)as the target value for all drying experiments was reached. Experiments were carried out with ultrasound application and without ultrasound (as control treatment) in three replications. Each experiment was conducted in combination of three ultrasound power density levels (11.1, 14.6 and 18.7 kW/m^3), four frequency levels (20, 25, 28 and 30 kHz) and three temperature levels (40, 50 and 60^{o}C). During the drying experiment, the sample moisture content was calculated through weighting it periodically with a digital balance (±0.01g, Max 2000g; EK-2000, AND, Japan). Dimensionless moisture ratio (*MR*) formula used for obtaining corn drying kinetics as follows [2-38]:

$$MR = \frac{M_t - M_e}{M_i - M_e} \quad (1)$$

Where M_t is moisture content at time t (decimal dry basis), $M_i$is the initial moisture content (decimal dry basis) and M_e is the equilibrium moisture content (decimal dry basis) obtained from Chung-Pfost equation:

$$M_e = E - F\ln[-(T+C)\ln(RH)] \quad (2)$$

Where T is the temperature (°C); C, E and F are 30.20, 0.34 and 0.06for shelled corn, respectively and RH is the relative humidity (decimal).

2.4. Statistical analysis

A factorial experiment was conducted in a completely randomized design (CRD) with three replications. Analysis of variance was performed using SAS software, version 9.0. The Duncan's multiple range test with a significance level of 5 % was applied to determine significant differences between the treatments.

2.5. Quality evaluation

2.5.1. Mechanical properties

After each drying experiment, the qualitative characteristics including ultimate compressive strength and toughness of dried corn was determined for 20 kernels using an Instron Universal Testing apparatus or Texture Analyser machine(STM-20, SANTAM, Iran; Figs. 3a and 3c) equipped with a load-cell (DBBP-50, Taiwan; Figs. 3a and 3d) having a rated capacity of 50kgf,the compression force being applied at a rated output of 0.51 mm/min and a probe with for the spherical indenter used consisted of a steel ball, with a diameter of ≅ 1.7 mm used for corn (Figs. 3a and 3b)[2-39].The changes in displacement versus force caused by penetration of the probe into the corn sample were plotted on a computer. The probe penetration continued until the force reached to the maximum value and sample started to rupture and the curve dropped and eventually the experiment was ended. This maximum force was the ultimate compressive strength. When the test was finished the area under the curve (just before sample rupture) was calculated using MATLAB 2013a software. Toughness was obtained from the area divided by the sample volume. 20 subsamples of corn kernels were taken randomly and length (*L*), width (*W*) and thickness (*T*) of seeds were measured using a digital caliper with an accuracy of 0.01 mm. Equivalent diameter (d_e) and volume (V_e) of corn kernels were found by analogy with a sphere of the same geometric mean diameter, using the following equations [40-41]:

$$d_e = (LWT)^{1/3} \quad (3)$$

$$V_e = \frac{1}{6}\Pi d_e^6 \quad (4)$$

For Peer Review Only

2.5.2. Image segmentation and Feature extraction

To determine the quality of shelled corns before and after each test, some photos were taken from samples which were later used for processing and analysis. To do this before and after each run three 36-corn sets were randomly chosen from drying chamber and then arranged in a specific chamber with indirect lighting called ''cloudy sky'' for photographing [12,42] (Fig. 4). To avoid variations in the quality of pictures for image processing the light was shined steadily and indirectly. The chamber was protected from outdoor light and illuminated using four halogen lamps with a continuous DC electric power supply. Three photos were taken from each 36-corn sample using a digital CCD camera (Canon IXUS 960IS, 12.1 megapixel camera with 3.7x optical zoom lens; Canon Inc, Tokyo, Japan) which was mounted vertically at the distance of 30 cm over the samples [12-42].The images having highest quality and resolution were selected for analysis. They were then transferred to a PC for further processing using MATLAB R2013a software. Certain MATLAB commands were employed to extract shape features. A computer algorithm which determines length, width and projected area of a grain kernel, can provide a basic analytical tool for quantifying shape. An algorithm was developed to determine the major and minor diameters (length and width) of corn. The original approach was to position kernels so that the major diameter was always parallel or perpendicular to the horizontal rows of pixels from the camera. A subsequent algorithm was developed that measured major diameter independent of kernel orientation. This algorithm used a threshold to distinguish an object from the background, producing a binary image. Next, an algorithm commonly referred to as the principal component was used to find the orientation of two vectors, which passed through the centroid of the object. The covariance matrix of the two-dimensional image vector was calculated. The eigenvectors of the covariance matrix pointed in orthogonal directions of maximum variance, passing through the centroid of the image. One of these vectors defined the line representing the length of the object, while the second defined the perpendicular distance passing through the centroid of the object. For corn kernels the length was measured longitudinally along the kernel tip cap to the crown and was defined as the major axis. The "width" determined by the orientation algorithm was not a true width; but was defined as a lone perpendicular to the major axis which also passed through the centroid of the object. Projected area was determined by counting the number of pixels contained in the binary image of the kernel. After calibration, the lens aperture, focus, and distance to the viewed object were maintained constant. The kernels were viewed under the camera, and pixels were counted along the length of the kernel[43].Surface area, perimeter, maximum diameter, minimum diameter and equivalent diameter were directly determined from each image and if the shrinkage in volume equals to the volume of water lost by evaporation during all the stages of the drying, the change of the surface area of corn with shrinkage is indicated in the following equation (Eq.7)[43]. Since the surface area is proportional to two-thirds power of the volume, the surface area as a proportion of the initial surface area has to be expressed in equation (Eq. 7) [40-44]. The initial surface area (A_o) and initial volume (V_o) of corn kernels were found by the equation Eq. 5 and 6 respectively [45,46,47,48,49]. Subsequently, shrinkage was calculated and evaluated using Eq. 8.

$$A_o = \pi d_e^{\,2} \quad (5)$$

$$V_o = \frac{1}{6}\Pi d_e^{\,6} \quad (6)$$

$$\frac{A}{A_o} = \left(\frac{V}{V_o}\right)^{\frac{2}{3}} \quad (7)$$

For Peer Review Only

$$\text{Shrinkage } \% = \frac{V_o - V}{V_o} \times 100 \quad (8)$$

The data obtained from MATLAB were in pixels which then were converted into millimeters. The data were directly imported from MATLAB to Excel software (2010). Statistical analysis was carried out by SAS 9.0 software as the second step. In order to evaluate color changes the images were analyzed in the RGB (i.e. Red, Green and Blue) and $L^*a^*b^*$ space by means of MATLAB software [12-50]. L^* is the luminance or lightness component, which ranges from 0 to 100 ($L^* = 0$ yields black and $L^* = 100$ indicates diffuse white) and parameters a^* (from green to red) and b^* (from blue to yellow) are the two chromatic components, which range from -120 to 120 [51, 52, 53, 54, 55]. Usually, the color of foods has been measured in $L^*a^*b^*$ and the most often used color model is the RGB model in which each sensor captures the intensity of the light in the red (R), green (G) or blue (B) spectrum, respectively [56].

2.6. Neural Networks

Drying time and moisture content variation in the ultrasound-assisted fluidized bed dryer and quality factors of the product (ultimate compressive strength and toughness) were modeled using ANNs. In Artificial Neural Networks (ANN) research, most efforts have centered on the development of new learning rules, the exploration of new neural network architectures and the expansion of new fields of application. Not much attention has been dedicated to the development of procedures that would permit the understanding of the nature of the internal representations generated by the network to respond to a given problem. Instead, ANN have been presented to the user as a kind of 'black box' whose extremely complex work transforms inputs into predetermined outputs [57].ANN, a computational approach inspired by biological neural networks of human is an appropriate tool to estimate functions where the complex relations between large number of input and output data are being modeled [58]. In the first step of ANN modeling the collected data are divided into three sets. The first set is used for training the network, the second for validating the model and the third one for testing the model. Each network contains three main layers including input, output and hidden layers. Through processing nodes information is transferred between the layers. When developing the network data are received, saved and manipulated in each node of a given layer and then passed to the nodes in the next layer [59]. It is not possible to find out immediately how the weights of the network or the activation values of the hidden neurons are related to the set of data being handled. Thus, unlike classic statistical models, in a network it does not appear to be easy to find out the effect that each explicative variable has on the dependent variable. The different methods have been proposed for interpreting what has been learned by a feed forward neural network composed of input neurons, hidden neurons, and output neurons. As shown in Fig. 5, these interpretative methods can be divided in two types of methodologies: analysis based on the magnitude of weights and sensitivity analysis. Analysis based on the magnitude of weights groups together those procedures that are based exclusively on the values stored in the static matrix of weights to determine the relative influence of each input variable on each one of the network outputs [57].In the beginning of training phase node weights are initialized with random values. Using either steepest-gradient descent principle or generalized delta rule the weights are frequently modified or updated. Once a termination criterion is satisfied the training process converges. It may also happen provided that there is not any significant change in the values corresponding to the connection links. In this study 70% of the data were randomly selected to train the ANN model, 15% to validate and the remaining 15% to test the network performance. To avoid over-training, the training process stopped by set training parameters and validation check as soon as the error of test data was about to rise similar to the previous work [12]. In order to check how good the developed model was mean square error (MSE) and coefficient of determination (R^2) were calculated. The model with

URL: http:/mc.manuscriptcentral.com/ldrt Email: mpeasm@nus.edu.sg

For Peer Review Only

the lowest MSE and the highest R^2 was introduced as a well-designed model [60].The methodology used for the assessment of network performance involves obtaining the minimum statistical measures of error between experimental and predicted transient time predicted by the model. In this study, statistical parameters namely, mean absolute error (*MAE*), mean square error (*MSE*), Mean relative error (*MRE*) and correlation coefficient (R^2) represented by Eqs. (9)–(12) were computed to check the performance of the developed model [60-61].

$$MAE = \frac{1}{N}\sum_{i=1}^{N}\left|T_{exp,i} - T_{ANN,i}\right| \quad (9)$$

$$MSE = \frac{1}{N}\sum_{i=1}^{N}\left(T_{exp,i} - T_{ANN,i}\right)^2 \quad (10)$$

$$MRE = \left[\frac{\frac{1}{N}\sum_{i=1}^{N}\left|T_{exp,i} - T_{ANN,i}\right|}{T_{exp,i}}\right] \quad (11)$$

$$R^2 = \left[1 - \frac{\sum_{i=1}^{N}\left(T_{exp,i} - T_{ANN,i}\right)\left(T_{exp,i} - T_{ANN,i}\right)}{\sum_{i=1}^{N}\left(T_{ANN,i}\right)\left(T_{ANN,i}\right)}\right] \quad (12)$$

In these equations, $T_{exp,i}$and $T_{ANN,i}$ are the average experimental and calculated parameters for the *i*th observation, respectively and *N* is the number of observations. A well trained ANN model should produce small MAE, MSE and MRE with large R^2 values [11, 12, 60, 61].

The Neural Network Toolbox of MATLAB software was used for ANN modeling. The classical back propagation algorithm was used to train the network. For the hidden layers to reach the optimum number of neurons different number of neurons together with two randomly selected transfer functions (Tansig: Hyperbolic tangent sigmoid and Logsig: Log sigmoid) and two algorithms (Trainscg: Scaled conjugate gradient, and Trainlm: Levenberg–Marquardt) were used to train the developed ANN model. One of the most difficult tasks in ANN model development is finding the optimal network architecture. This network architecture can be selected out of several network configurations containing the combination of various model parameters namely, the number of neurons in the hidden layers, different transfer functions and the training algorithms. A list of different transfer functions and training algorithms investigated during training network is summarized in Table 1. In order to obtain the optimum number of neurons in the hidden layer for each of sample geometry, the ANN model was trained with varying numbers of neurons and randomly chosen. The number of selected neurons has great effect on the model prediction performance [11].For the four networks with output predictions of drying time, moisture content, toughness and ultimate compressive strength the inputs were chosen as drying air temperature, frequency and ultrasound power density whereas for the network which predicted output, two input hidden layers were added. Fig. 6 depicts the schematic structure of the applied neural network with its three inputs; two hidden layers, and single output layer. Initially, the performance of ANN model was assessed with a given number of neurons with a randomly chosen transfer function and the training algorithms. In order to study the effect of different parameters on network performance, the model was run by changing an important involving parameter and keeping the others parameters constant. The iteration process of performance assessment was continued until the most appropriate model for simulating the experimental values with highest correlation coefficient of determination and least values in errors was obtained [11].

2.7. Specific Energy Consumption (SEC)

The other purpose of the present study was to select the best treatment to have optimum drying process considering specific energy consumption. The amount of energy needed to remove one kilogram of water from the product is called SEC and can be calculated according to the following Eq.(13). It depends on the design of the dryer, initial temperature and moisture content of kernel, the bed thickness, the amount of moisture removed, weather conditions during drying, the

URL: http:/mc.manuscriptcentral.com/ldrt Email: mpeasm@nus.edu.sg

For Peer Review Only

drying air temperature and mass flow rate. Since reducing drying cost involves minimizing specific energy consumption, the specific energy consumption was discussed as optimization criterion. Generally, three types of energy were consumed in the drying process. First the energy required to drive the fan for introducing air flow into the dryer bed, second the energy needed for heating up the inlet air and finally the energy required for ultrasound generator.

$$SEC = \frac{E_t}{m_{ev}} \quad (13)$$

Where E_t is the total energy consumption (J) and m_{ev} is the total amount of water evaporated from corn over the drying process (kg).The centrifugal fan power needed to blow the air per unit area of the bed can be calculated as follows:

$$FP = \frac{\Delta p v_a}{\eta_f} \quad (14)$$

Where FP is the centrifugal fan power (W), Δp is the total pressure drop (Pa), v_a is the inlet air velocity (m/s), η_f is the centrifugal fan efficiency which depends on the fan type and the wide-open volume percentage and considered to be 0.5 according to corresponding curves [2].Three parameters could affect the total pressure drop and fan power (Δp), including static pressure owing to seeds resistance (Δp_g), the pressure drop induced by pipes and ducts conveying air (Δp_d) and the perforated seed-bed resistance which was neglected because the perforated area was more than 10% of the whole surface area [2-62]. Therefore total pressure drop defined as fallow:

$$\Delta p = \Delta p_g + \Delta p_d \quad (15)$$

This pressure drop resulted from clean seeds with the thickness of L (m) was calculated as fallows[2]:

$$\Delta p_g = \frac{5.38 \times 10^4 \times L \times V_a^2}{Ln(1 + 79V_a)} \quad (16)$$

The pressure drop due to direction change (Fig. 7) was determined by Eq. (17) [2-63]:

$$\Delta p_d = c_2 (\frac{V_a}{1.29})^2 \quad (17)$$

And $c_2$was considered to be 0.19.

The electric thermal power required for heating up the drying air was calculated by the heat balance equation as follows:

$$HP = \rho_d V_a C_p (T_d - T_a) \quad (18)$$

Where ρ_a is air density (kg/m^3), C_p is air specific heat capacity (J/kg·K), T_d and T_a are the inlet drying air and the ambient air temperatures (K), respectively. The ultrasound power (UP) can be calculated as follows:

$$UP = UI\cos\Phi \quad (19)$$

Where U (V) and I (A) are the voltage and electric current, respectively consumed by the ultrasound generator and cosΦ is the power factor considered to be 0.8. Total energy consumption was obtained from the following equation:

$$E_t = [(FP + HP)A + UP]\Delta t \quad (20)$$

URL: http:/mc.manuscriptcentral.com/ldrt Email: mpeasm@nus.edu.sg

For Peer Review Only

Where A is cross sectional area of drying bed (m^2) and Δt is final drying time (s).

3. Results and Discussion

3. 1. Drying kinetics

3.1.1. Drying time

A range of frequencies were applied in different power densities, in other to study the effect of high power ultrasound on drying time. For each treatment, the final drying time were calculated and are shown in Table 2 and Table 3 summarizes the variance analysis for the effect of different drying factors i.e., drying air temperature (T), frequency (F), ultrasound power density (P) on drying time at 1% probability level. As can clearly be seen, drying duration was influenced by inlet air temperature, frequencies and power densities. All interactions were also significant which means the effects of different factors on drying time were different. Figs. 8 and 9 illustrate the effects of inlet air temperature, frequency and power density on final drying time. The Duncan test at 5% of probability was applied to determine significant differences between treatments. As can be observed in Fig. 8, by increasing temperature in fluidized bed modes the drying time decreased significantly that the same behaviors were observed and reported by Özahi and Demir [64, 65, 66]. The least drying time was observed at drying air temperature of 40°C, frequency of 25 kHz and ultrasonic power density of 14.6 $kW/m^3$and drying time was reduced up to 43% compared to that of the control (without ultrasound). Also it can be observed that frequency of 25kHz in comparison with other frequencies had the most significant influence on reduction of final drying time. It is clear from Fig.8 that by increasing drying air temperature for all treatments including fluidized bed only (control treatments) and ultrasound-assisted fluidized bed drying, drying time reduced. One important issue need to be considered is that the effect of each frequency at each temperature level should be compared with its control values (no ultrasound).

At drying air temperatures of 50°C and 60°Cthere was no significant difference among different frequency levels and somehow the final drying time increased when frequency increases. This is due to the fact that increasing drying air temperature in drying process causes greater cell damages, especially when samples were subjected to ultrasound treatment. Moreover, ultrasound is a mechanical wave which can penetrate in denser air (lower temperature) and subsequently into the grain (air-borne ultrasound drying).The lower frequencies have better penetrations at lower temperatures. Therefore increasing the inlet drying air temperature diminished the effect of ultrasound on dehydration process. Finally, as presented in Fig. 9, drying rate was increased at power density (14.6kW/m^3) and the drying time was shortened at the power density compared to the control group. It might be due to the fact that the greater part of the ultrasonic waves was damped at lower power densities. Furthermore, no significant difference was observed among drying time for different power densities at drying temperature of 50°C and 60°C as by increasing temperature the effect of ultrasound on drying time reduces. This is due to the fact at higher temperature levels ultrasound had a negative effect on moisture removal as a result of distortion of particular parenchyma cells and consequently caused a higher drying time. Other researchers reported that the influence of ultrasound on drying rate is more obvious at lower temperature. The higher efficiency of the ultrasound-assisted air drying at lower temperatures is caused by the additional energy provided by ultrasound during drying [67].Also the effect of ultrasound power on drying rate decreases with the reduction of samples' moisture content during drying process [68].

3.1.2. Moisture ratio

The moisture ratio values are plotted in Figs.10 and11at different frequency and power density levels respectively for the most effective drying air temperature of 40°C. Fig. 10 shows that different frequencies had different effect on drying curves in the most effective combination of temperature (40°C) and power density(14.6 kW/m^3) on final drying time. The

URL: http:/mc.manuscriptcentral.com/ldrt Email: mpeasm@nus.edu.sg

For Peer Review Only

drying curve for the frequency of 20kHz approached to the control treatment. In other word this frequency had no effect on drying rate. As can be observed from drying curves, the frequency of 25 kHz is the most effective frequency on drying rate. At this frequency the slope of the graph is greater than the others, which indicates moisture loss was greater than others and as a result the final drying time was shorter compare to the other frequencies. Also in Fig.11 all of power densities were evaluated in the most effective temperature (40^{o}C) and frequency (25 kHz) on final drying time. Drying rate declined at lowest power density of 11.1kW/m^{3}as represented in Fig.11. Whereas drying curves for power densities of 14.6 kW/m^3 and 18.7 kW/m^3 were close to each other and there was a gap between these two curves and the rest. The effect of HPU disappeared at the lowest ultrasonic power level. The results of the experiment were similar to those reported by other researchers[31,69, 70, 71].

3.2. Quality aspects

3.2.1. Ultimate compressive strength and toughness

The ANOVA result for the ultimate compressive strength of corn kernels is presented in Table 4 for all the drying variables (T, F, and P). It was observed that drying air temperature and frequency had significant effect on compressive strength of corn kernels whereas ultrasound power density had no significant effect on compressive strength. Fig. 12 shows the mean differences of compressive strength for the interaction of frequency and drying air temperature (Duncan test, at 5% probability). It is clear from Fig. 12that higher temperature caused a significant decrease in compressive strength of kernels as the higher the drying temperature produce more damage to the tissue cells of corn structure and result in more frangible corn kernels in fluidized bed mode (control treatments). Other researchers by aid of computer simulations of drying kernels showed that removal of water from the region adjacent to the surface caused a tensional stress in that region, and a compression stress in the center of the kernels [72] and the tensile strength or maximum stresses are greater than the compressive ones, thus fracturing or brittle damage occurs near the boundary of dried materials [73]. At drying air temperature of 40^{o}C and frequency of 28 and 30kHz,the compressive strength of corn kernels decreased by almost28.36% and 29.62% compared to the corresponding values of the control sample because samples were subjected to more time of ultrasound and a longer ultrasound treatment time resulted in greater destruction of structure of dried corn, moreover application of ultrasound at higher frequencies cause vigorously cell damage. However, at drying air temperature of 50 and 60^{o}C there was no significant difference observed in compressive strength of corn kernels among HPU groups when compared with its control value. The same behavior was observed by Nowacka et al.[25] during rehydration of apple by ultrasound pretreatment. The result of ANOVA for the toughness of corn kernels is presented in Table 5. It is shown that all the drying variables had significant effects on toughness of kernels except the ultrasound power density. As it is shown in Fig.13,increasingdrying air temperature caused a significant decrease in toughness of kernels in the fluidized bed mode (control treatments). This is due to the fact the higher temperature causes higher moisture and temperature gradient in the corn kernels and subsequently the fissure appears in the kernels. The least toughness belonged to drying air temperature of 40^{o}C and frequencies of 28 and 30 kHz which showed a reduction of 79.66 and 79.23% respectively in toughness value when compared with its control value. As a result increasing temperature during drying has severe effect on corn structure and cause cell damage of corn kernels especially when samples were exposed to more time of ultrasound treatment having higher frequencies. This demonstrates a close relation between the required mechanical strength of corn kernel and its exposure duration to the thermal and ultrasonic treatments. These results agreed with those attained by other investigators [19,74,25].Based on the results of ultimate compressive strength and toughness of corn kernels, it can be said that application of ultrasound caused breaking down of cells and disruption of contiguous cells which produced large cell interspaces and subsequently reduced required force

URL: http:/mc.manuscriptcentral.com/ldrt Email: mpeasm@nus.edu.sg

For Peer Review Only

and energy needed to rupture the samples. Even though the samples were selected carefully in size and shape, during compressing test for some kernels the bio-yield point and the rupture points coincided so that they could not be distinguished clearly. Most food and biological materials exhibit non-linear behavior at larger (e.g., 5% strain or greater) deformations and have viscoelastic behavior [39]. In addition some changes may occur in the properties of dried material after ultrasound treatment. Therefore the toughness modulus which is the area under the stress-strain curve up to the rupture point gave better results than ultimate compressive strength in the experiments and it was more appropriate index representing the grain hardness and quality.

3.2.2. Shrinkage

Table 6 presents the analysis of variance at the probability level of5%, for the effect of different drying variables on shrinkage of dried samples. The effect of drying air temperature (T), frequency (F) and ultrasound power density (P) on shrinkage was not significant. However, only the interaction of inlet air temperature and frequency on shrinkage was significant ($p<0.5$). Fig.14 illustrate the effects of inlet air temperature and frequency on shrinkage. The highest shrinkage value was observed at drying air temperature of 40^{o}C and frequencies of 28 and 30kHz which led to a reduction of 12.73% and 13.13% respectively in volume of corn kernels whereas there was no significant difference between the effect of drying air temperatures of 50 and 60^{o}C in comparison with its control values.

The density and shrinkage of maize dried in a fluidized bed dryer will depend particularly on the moisture content of the final product[75]. Depending on drying method and parameters such as temperature and air flow, both the amount of shrinkage and the degree of damage to interior structure of product cells are liable to change[76].According to Fig.14, at drying air temperature of 40^{o}C and frequencies of 28 and 30kHz, shrinkage was significantly different from other treatments due to the longer duration of the drying in these treatments. Although ultrasound has non-thermal character as the subsidiary factor, it plays an important role in duration of final drying time.

3.2.3. Color specification

3.2.3.1. RGB color measurement

Fig. 15 illustrates the effects of inlet air temperature and frequency on RGB components of corn color. The effect of ultrasound power density on the RGB components was not significant. The Duncan test was performed to determine any significant differences between treatments. Color changes of samples in ultrasound-assisted fluidized bed drying treatments were higher compared to its control value (fresh corn). By increasing the temperature and frequency the quality of the color reduced as RGB components of corns increased in comparison with fresh corn (control),implying that the corn had become whiter and brighter. Color is an important quality sign resulting from the interplay of light the object and the observer. Similar studies investigated the effect of conventional drying method on the color of dehydrated products and reported that all morphological features decreased smoothly during drying[36,77,78]. Since, drying of cellular tissues generally produces physical (color, texture, shape, porosity and etc.) changes[79,80,81,82] and a long-lasting hot air drying may result in a significant change in color alteration and destruction of natural dyes in product. The color of a natural pigment is unstable and sensitive to various factors such as light, temperature and etc. Thus, application of ultrasound affecting the duration of drying time led to a color change proportional to duration of drying time. Since heat is the most effective factor on changing color of the corn when the drying time decreased the values of RGB remained constant compared to those of the fresh corn.

3.2.3.2. $L^{*}a^{*}b^{*}$ color measurement

URL: http:/mc.manuscriptcentral.com/ldrt Email: mpeasm@nus.edu.sg

For Peer Review Only

According to Duncan's multiple rang test, the effect of different drying air temperatures and frequencies on $L^*a^*b^*$ components was shown in Fig. 16. The effects of ultrasound power density on $L^*a^*b^*$components of corn color was not significant. In the $L^*a^*b^*$ color space, the two components of a^* and b^* underwent significant changes, but L^* which represents the luminance of images did not. As was mentioned previously, the illumination was kept constant in the sky chamber when photos were taken, so that the images were taken with a uniform light quality. By increasing the temperature and frequency a^* and b^* went to positive values. Color changes of samples dried in ultrasound-assisted fluidized bed drying treatment were higher compared to hot air (fluidized bed). Similar results was also found by aid of colorimeter and expressed in CIE $L^*a^*b^*$color space (precision 0.01) of drying apples that showed color changes of samples dried in ultrasonically aided convective drying schedules (CV-US) were higher compared to convective (CV) ones [83]. However at the drying air temperature of 40°C, a^* and b^* values did not change significantly and colors changes from green to red (a^*) and blue to yellow (b^*) were very low and the negative values declined. Average colors changes at the drying air temperature of 40°C were less than those of 50 and 60°C, Therefore at the lower frequency and lower temperature the color component of shelled corn varied less and an acceptable quality level was preserved.

3.3. Assessment of ANN prediction

The results of ANN modeling for prediction of moisture content, drying time, toughness and ultimate compressive strength of shelled corn were strongly dependent on input parameters. Similar results were reported by Tripathy and Kumar [84]. Among tested ANN topologies, those with the lowest MSE and highest coefficient of determination were introduced as the best. However, ANN modeling for prediction of ultimate compressive strength was not compatible with all results (the highest MSE and lowest coefficient of determination) thus it could not be modeled. This may due to the fact that the bio-yield and the rupture points on the stress-strain curve coincided and thus they could not be distinguished clearly for the ultrasound-dried corn kernels. Performance of the network in prediction of moisture content, drying time and toughness was evaluated by plotting the predicted values against the experimental data. Typical plots comparing experimental and predicted values of drying time during training, validation and testing of the selected ANN model is presented in Fig. 17. From Fig.17 it is observed that the best model is the one with highest R^2, in training, validation and testing as well as all data together. The best ANN topology for the drying time model was 3-14-15-1(number of neurons) with transfer function of tansig and lowest MSE of 9.14 which was obtained after 3 training cycles as is shown in Table 7. Furthermore, the best ANN models for moisture content and toughness, were also obtained and presented in Table 7 with related validation indices. The results of this study suggest that the ANN modeling technique could effectively be applied in prediction of the drying parameters similar to the results reported by Momenzadeh et al. [11],Khawas et al [85]Barzegar et al. [12]and Aghbashlo et al.[86].

3.4. Specific Energy Consumption (SEC)

The maximum reduction of SEC respect to its control value belonged to the treatment with temperature of 40°C, frequency of 25 kHz and power density of 14.6 kW/m^3(Table8).For this treatment the SEC reduced about 32% when compared with its control. However, the SEC increased at temperature of 50 and 60°C when ultrasound treatment was applied. This is due to the fact at higher temperature levels ultrasound had a negative effect on moisture removal as a result of distortion of particular parenchyma cells and consequently caused a higher drying time and energy consumption.

3.5. Selection of the Drying Process

The optimum drying condition was determined based on both specific energy consumption and quality of dried corns. The grain quality attributes depend on final product utilization for food or feed. If the grain is planned to be milled for

URL: http:/mc.manuscriptcentral.com/ldrt Email: mpeasm@nus.edu.sg

For Peer Review Only

animal feeding, it is desirable to have lower toughness so that lower energy will be required for grinding. Based on toughness results presented in Fig.13, the sponge effect caused by ultrasound application led to reduction of toughness of corn kernels. To select the best treatment, a compromise should be made between final quality of the grain and the amount of energy consumed in drying process. Therefore, the treatment with temperature of 40°C, frequency of 25 kHz and power density of 14.6 kW/m^3 was introduced as the best selection for ultrasound-assisted fluidized bed drying.

4. Conclusions

Based on the results, it can be concluded that drying time and specific energy consumption of corn drying decreased significantly when lower frequencies and lower drying temperatures (e.g. 40°C) is applied in process of HPU fluidized bed drying. The quality of the grain including compressive strength, toughness, color parameters and shrinkage is highly influenced by drying parameters. The treatment having the frequency of 25 kHz and power density 14.6 kW/m^{3}wasthe most treatment on drying time and caused 43% reduction in drying duration in comparison with no ultrasound (control).

Considering drying kinetics, quality and energy factors the optimum drying condition was selected to be the treatment having drying air temperature of 40°C, frequency of 25kHz and power density of 14.6 kW/m^3.

The most accurate predictions for drying time, toughness and moisture content were attained by the mentioned ANN models using Logsig and Tansig transfer function with trainscg and trainlm back propagation algorithm.

Nomenclature

A	Drying bed surface area (m^2)
ANN	Artificial neural network
c_p	Specific heat capacity of air (J/kg.K)
c_2	90-Degree round section pressure loss coefficient
E, F, C	Corn-specific empirical constants
E_t	Energy consumption(J)
FP	Power supplied to the fan per unit area of the bed (W)
HP	Power consumption of air heaters per unit area of the bed (W)
I	Electrical current (A)
L	Corn bed thickness (m)
m_{ev}	Evaporated water from grains (kg)
MR	Moisture ratio (dimensionless)
M_t	Moisture content of corn at time t (decimal)
M_i	Initial moisture content (decimal)
M_e	Equilibrium moisture content (decimal)

URL: http:/mc.manuscriptcentral.com/ldrt Email: mpeasm@nus.edu.sg

For Peer Review Only

MSE	Mean square error
MAE	Mean absolute error
MRE	Mean relative error
ΔP	Total pressure drop of drying air (Pa)
ΔP_d	Pressure drop of air due to the duct system (Pa)
ΔP_g	Pressure drop of air due to the perforated bed (Pa)
R^2	Coefficient of determination
RH	Relative humidity (decimal)
HPU	High power ultrasound
RGB	Red, Green, Blue
a^*	Rate of color change from green to red
b^*	Rate of color change from blue to yellow
L^*	Luminance of image
ANN	Artificial neural networks
SEC	Specific energy consumption
T_a	Ambient temperature (K)
T_d	Inlet air temperature (K)
U	Voltage (V)
v_a	Inlet air velocity (m/s)
V_1	Initial volume of product (m^3)
V_2	Final volume of product (m^3)
ρ_a	Air density(kg/m^3)
$\cos\phi$	Power factor (dimensionless)
η_f	Fan efficiency (dimensionless)

For Peer Review Only

References

[1] FAO, 2014. Food and Agriculture Organization of the United Nations Statistics Division, accessed at: <www.faostat.fao.org>.

[2] Brooker, D. B.; Bakker-Arkema, F. W.; Hall; C. W. *Drying and storage of grains and oilseeds*; Van Nostrand Reinhold: New York, 1992.

[3] Zare, D.; Minaei, S.; Zadeh, M. M.; Khoshtaghaza, M. H. Computer simulation of rough rice drying in a batch dryer. *Energy Conversion and Management***2006**, *47*(18), 3241-3254.

[4]Zare, D.; Jayas D. S; Singh, C.B. A generalized dimensionless model for deep bed drying of paddy. *Drying Technology***2012**, 30(1) 44-51.

[5] Ranjbaran, M.; Emadi, B.; Zare, D. CFD simulation of deep-bed paddy drying process and performance. *Drying Technology***2014**, *32*(8), 919-934.

[6] Ranjbaran, M.; Zare, D. CFD modeling of microwave-assisted fluidized bed drying of moist particles using two-fluid model. *Drying Technology***2012**, *30*(4), 362-376.

[7] Zare, D.; Ranjbaran, M. Simulation and validation of microwave-assisted fluidized bed drying of soybeans. *Drying Technology***2012**, *30*(3), 236-247.

[8] Ranjbaran, M.; Zare, D. Simulation of energetic-and exergetic performance of microwave-assisted fluidized bed drying of soybeans. *Energy***2013**, *59*, 484-493.

[9] Menon, A. S.; Mujumdar, A. S.; *Drying of solids: principles, classification, and selection of dryers*; Marcel Dekker Co.: New York, 1995; 1-39.

[10] De la Fuente-Blanco, S.; De Sarabia, E. R. F.; Acosta-Aparicio, V. M.; Blanco-Blanco, A.; Gallego-Juárez, J. A. Food drying process by power ultrasound. *Ultrasonics***2006**, *44*, e523-e527.

[11]Momenzadeh, L.; Zomorodian, A.; Mowla, D. Experimental and theoretical investigation of shelled corn drying in a microwave-assisted fluidized bed dryer using Artificial Neural Network. *Food and Bioproducts Processing***2011**, *89*(1), 15-21.

[12] Barzegar, M.; Zare, D.; Stroshine, R. L. An integrated energy and quality approach to optimization of green peas drying in a hot air infrared-assisted vibratory bed dryer. *Journal of Food Engineering***2015**, *166*, 302-315.

[13] Jafari, A.; Zare, D. Ultrasound-assisted fluidized bed drying of paddy: Energy consumption and rice quality aspects. *Drying Technology***2017**, *35*(7), 893-902.

[14] Abdoli, B. Evaluation of corn drying process in an ultrasound-assisted fluidized bed dryer. Unpublished MS. Thesis, Shiraz University, Shiraz, Iran, 2016.

[15] Gallego-Juárez, J. A.; Riera, E.; De la Fuente Blanco, S.; Rodríguez-Corral, G.; Acosta-Aparicio, V. M.; Blanco, A. Application of high-power ultrasound for dehydration of vegetables: processes and devices. *Drying Technology***2007**, *25*(11), 1893-1901.

[16] Cárcel, J. A.; García-Pérez, J. V.; Riera, E.; Mulet, A. Influence of high-intensity ultrasound on drying kinetics of persimmon. *Drying Technology***2007**, *25*(1), 185-193.

[17] Jambrak, A. R.; Mason, T. J.; Paniwnyk, L.; Lelas, V. Accelerated drying of button mushrooms, Brussels sprouts and cauliflower by applying power ultrasound and its rehydration properties. *Journal of Food Engineering***2007**, *81*(1), 88-97.

[18] Fernandes, F. A.;Rodrigues, S. Ultrasound as pre-treatment for drying of fruits: Dehydration of banana. *Journal of Food Engineering***2007**, *82*(2), 261-267.

For Peer Review Only

[19] Fernandes, F. A.; Gallão, M. I.; Rodrigues, S. Effect of osmotic dehydration and ultrasound pre-treatment on cell structure: Melon dehydration. *LWT-Food Science and Technology***2008**, *41*(4), 604-610.

[20] Fernandes, F. A.; Rodrigues, S. Dehydration of sapota (Achrassapota L.) using ultrasound as pretreatment. *Drying Technology***2008**, *26*(10), 1232-1237.

[21] Karki, B. Use of high-power ultrasound during soy protein production and study of its effect on functional properties of soy protein isolate. Unpublished Ph. D. Dissertation, Iowa State University, Ames. 2009.

[22] García-Pérez, J. V.; Cárcel, J. A.; Riera, E.; Mulet, A. Influence of the applied acoustic energy on the drying of carrots and lemon peel. *Drying Technology***2009**, *27*(2), 281-287.

[23] Fernandes, F. A.; Gallão, M. I.; Rodrigues, S. Effect of osmosis and ultrasound on pineapple cell tissue structure during dehydration. *Journal of Food Engineering***2009**, *90*(2), 186-190.

[24] Garcia-Noguera, J.; Oliveira, F. I.; Gallão, M. I.;Weller, C. L.; Rodrigues, S.; Fernandes, F. A. Ultrasound-assisted osmotic dehydration of strawberries: Effect of pretreatment time and ultrasonic frequency. *Drying Technology***2010**, *28*(2), 294-303.

[25] Nowacka, M.; Wiktor, A.; Śledź, M.; Jurek, N.; Witrowa-Rajchert, D. Drying of ultrasound pretreated apple and its selected physical properties. *Journal of Food Engineering***2012**, *113*(3), 427-433.

[26] Schössler, K.; Jäger, H.; Knorr, D. Novel contact ultrasound system for the accelerated freeze-drying of vegetables. *Innovative Food Science & Emerging Technologies***2012**, *16*, 113-120.

[27] Szadzińska, J.; Łechtańska, J.; Kowalski, S. J.; Stasiak, M. The effect of high power airborne ultrasound and microwaves on convective drying effectiveness and quality of green pepper. *UltrasonicsSonochemistry***2017**, *34*, 531-539.

[28] Chen, Z. G.; Guo, X. Y.; Wu, T. A novel dehydration technique for carrot slices implementing ultrasound and vacuum drying methods. *Ultrasonicssonochemistry***2016**, *30*, 28-34.

[29] Cárcel, J. A.; Benedito, J.; Rosselló, C.; Mulet, A. Influence of ultrasound intensity on mass transfer in apple immersed in a sucrose solution. *Journal of food engineering***2007**, *78*(2), 472-479.

[30] Garcia-Perez, J. V.; Cárcel, J. A., Benedito, J.; Mulet, A. Power ultrasound mass transfer enhancement in food drying. *Food and Bioproducts Processing***2007**, *85*(3), 247-254.

[31] Rodríguez, Ó.; Santacatalina, J. V.; Simal, S.; Garcia-Perez, J. V.; Femenia, A.; Rosselló, C. Influence of power ultrasound application on drying kinetics of apple and its antioxidant and microstructural properties. *Journal of Food Engineering***2014**, *129*, 21-29.

[32] Tarleton, E.S. The role of field-assisted techniques in solid/liquid separation. Filtr. Separat. 29, 1992, 246-238.

[33]Tarleton, E.S.; Wakeman, R.J.; Povey, M.J.W.; Mason, T.J.;Ultrasounds in Food Processing; Blackie Academic and Professional; Glasgow, 1998.

[34] Sabliov, C. M.; Boldor, D.; Keener, K. M.; Farkas, B. E. Image processing method to determine surface area and volume of axi-symmetric agricultural products. *International Journal of Food Properties***2002**, *5*(3), 641-653.

[35] Louka, N.; Juhel, F.; Allaf, K. Quality studies on various types of partially dried vegetables texturized by controlled sudden decompression: General patterns for the variation of the expansion ratio. *Journal of Food Engineering***2004**, *65*(2), 245-253.

[36] Fernandez, L.; Castillero, C.; & Aguilera, J. M. An application of image analysis to dehydration of apple discs. *Journal of Food Engineering***2005**, *67*(1), 185-193.

[37] Menlik, T.; Özdemir, M. B.; Kirmaci, V. Determination of freeze-drying behaviors of apples by artificial neural network. *Expert Systems with Applications***2010**, *37*(12), 7669-7677.

URL: http:/mc.manuscriptcentral.com/ldrt Email: mpeasm@nus.edu.sg

For Peer Review Only

[38] ASABE Standards, ASAE S352.2; Moisture measurement- Ungrounded grain and seeds, St. Joseph, MI, USA, 2009. APR1988 (R2008b).

[39] ASABE Standards, ASAE S368.4; Compression test of food materials of convex shape, St. Joseph, MI, USA, 2009. DEC2000 (R2008a).

[40] Mohsenin, N.N. Physical Properties of Plant and Animal Materials, Gordon and Breach Science Publishers, New York, 1986.

[41] Abasi, S; Minaei, S. Effect of drying temperature on mechanical properties of dried corn. *Drying Technology***2014**, *32*(7), 774-780.

[42] Jafari, A.,; Bakhshipour, A. Inspection of quince slice dehydration stages based on extractable image features. *Czech J. Food Sci***2014**, *32*(5), 456-463.

[43] Paulsen, M. R.; Wigger, W. D., Litchfield, J. B.; Sinclair, J. B. Computer image analyses for detection of maize and soybean kernel quality factors. *Journal of Agricultural Engineering Research***1989**, *43*, 93-101.

[44] Suzuki, K.; Kubota, K.; Hasegawa, T.; Hosaka, H. Shrinkage in dehydration of root vegetables. *Journal of Food Science***1976**, *41*(5), 1189-1193.

[45] Sacilik, K.; Öztürk, R.; Keskin, R. Some physical properties of hemp seed. *Biosystems engineering***2003**, *86*(2), 191-198.

[46] Jain, R. K.; Bal, S. Properties of pearl millet. *Journal of Agricultural Engineering Research***1997**, *66*(2), 85-91.

[47] Tunde-Akintunde, T. Y., Akintunde, B. O. Some physical properties of sesame seed. *Biosystems Engineering***2004**, *88*(1), 127-129.

[48] Altuntaş, E.; Özgöz, E.,; Taşer, Ö. F. Some physical properties of fenugreek (Trigonellafoenum-graceum L.) seeds. *Journal of food Engineering***2005**, *71*(1), 37-43.

[49] Tarighi, J.; Mahmoudi, A.,; Alavi, N. Some mechanical and physical properties of corn seed (Var. DCC 370). *African Journal of Agricultural Research***2011**, *6*(16), 3691-3699.

[50] Poynton, C.A. Digital Video and HDTV. Algorithms and Interfaces. Morgan Kaufmann, USA, 2003.

[51] Papadakis, S. E., Abdul-Malek, S., Kamdem, R. E., & Yam, K. L.A versatile and inexpensive technique for measuring color of foods **2000**, *Food Technology*, *54*(12), 48-51.

[52] Segnini, S., Dejmek, P., Öste, R. A low cost video technique for colour measurement of potato chips. *LWT-Food Science and Technology***1999**, *32*(4), 216-222.

[53] Yam, K. L.; Papadakis, S. E. A simple digital imaging method for measuring and analyzing color of food surfaces. *Journal of Food Engineering***2004**, *61*(1), 137-142.

[54] Yam, K. L.; Papadakis, S. E. A simple digital imaging method for measuring and analyzing color of food surfaces. *Journal of Food Engineering***2004**, *61*(1), 137-142.

[55] Hunt, R. W. G. Colour standards and calculations. *The Reproduction of Colour, 6th Edition*, 2004.

[56] Hornberg, A. (Ed.). *Handbook of Machine Vision*. John Wiley & Sons,2007.

[57] Montano, J. J., Palmer, A. Numeric sensitivity analysis applied to feed forward neural networks. *Neural Computing & Application***2003**, *s*, *12*(2), 119-125.

[58] Çakmak, G.; Yıldız, C. The prediction of seedy grape drying rate using a neural network method. *Computers and Electronics in Agriculture***2011**, *75*(1), 132-138.

[59] Erenturk, S.; Erenturk, K. Comparison of genetic algorithm and neural network approaches for the drying process of carrot. *Journal of Food Engineering***2007**, *78*(3), 905-912.

For Peer Review Only

[60] Tripathy, P. P.; Kumar, S. Neural network approach for food temperature prediction during solar drying. *International Journal of Thermal Sciences***2009**, *48*(7), 1452-1459.

[61] Bakhshipour, A.; Jafari, A.; Zomorodian, A. Vision based features in moisture content measurement during raisin production. *World Appl. Sci. J***2012**, *17*(17), 860-869.

[62] Pabis, S.; Jayas, D.S.; Cenkowski, S. Grain drying: Theory and Practice, John Wiley & Sons, 1998.

[63] ASABE Standards, ASAE D272.3, Resistance to Airflow of Grains, Seeds, Other Agricultural Products, and Perforated Metal Sheets, St. Joseph, MI, USA, MAR1996 (R2007)

[64] Özahi, E.; Demir, H. A model for the thermodynamic analysis in a batch type fluidized bed dryer. *Energy***2013**, *59*, 617-624.

[65] Özahi, E.; Demir, H. Presentation of a test rig with its experimental procedure and uncertainty analysis of measurements for batch type fluidized bed drying of corn and unshelled pistachio nut. *Measurement***2014**, *53*, 117-127.

[66] Özahi, E.; Demir, H. Drying performance analysis of a batch type fluidized bed drying process for corn and unshelled pistachio nut regarding to energetic and exergetic efficiencies. *Measurement***2015**, *60*, 85-96.

[67] Fernandes, F. A., Rodrigues, S., García-Pérez, J. V., Cárcel, J. A. Effects of ultrasound-assisted air-drying on vitamins and carotenoids of cherry tomatoes. *Drying Technology***2016**, *34*(8), 986-996.

[68] Liu, Y.; Sun, Y.; Yu, H.; Yin, Y.; Duan, X. Hot air drying of purple-fleshed sweet potato with contact ultrasound assistance. *Drying Technology***2017**, 35(5), 564-576.

[69] Rodrigues, S; Gomes, M. C.; Gallão, M. I.; Fernandes, F. A. Effect of ultrasound-assisted osmotic dehydration on cell structure of sapotas. *Journal of the Science of Food and Agriculture***2009**, *89*(4), 665-670.

[70] Witrowa-Rajchert, D.; Rząca, M. Effect of drying method on the microstructure and physical properties of dried apples. *Drying Technology***2009**, *27*(7-8), 903-909.

[71] García-Pérez, J. V.; Cárcel, J. A.; De la Fuente-Blanco, S.;, De Sarabia, E. R. F. Ultrasonic drying of foodstuff in a fluidized bed: Parametric study. *Ultrasonics***2006**, *44*, e539-e543.

[72] Lewicki, P. P.; Jakubczyk, E. Effect of hot air temperature on mechanical properties of dried apples. *Journal of Food Engineering***2004**, *64*(3), 307-314.

[73] Ekstrom, G. A.; Lijedahl, J. B.; Peart, R. M. Thermal expansion and tensile properties of corn kernels and their relationship to cracking during. *Trans. ASAE***1966**, *23*(4), 556-561.

[74] Deng, Y., Zhao, Y. Effect of pulsed vacuum and ultrasound osmo pretreatments on glass transition temperature, texture, microstructure and calcium penetration of dried apples (Fuji). *LWT-Food Science and Technology***2008**, *41*(9), 1575-1585.

[75] Hatamipour, M. S.; Mowla, D. Correlations for shrinkage, density and diffusivity for drying of maize and green peas in a fluidized bed with energy carrier. *Journal of Food Engineering***2003**, *59*(2), 221-227.

[76] Lewicki, P. P.; Jakubczyk, E. Effect of hot air temperature on mechanical properties of dried apples. *Journal of Food Engineering***2004**, *64*(3), 307-314.

[77] Krokida, M. K.; Maroulis, Z. B.; Saravacos, G. D. The effect of the method of drying on the colour of dehydrated products. *International Journal of Food Science & Technology***2001**, *36*(1), 53-59.

[78] Ramos, I. N.; Silva, C. L.; Sereno, A. M.; Aguilera, J. M. Quantification of microstructural changes during first stage air drying of grape tissue. *Journal of Food Engineering***2004**, *62*(2), 159-164.

[79] Del Valle, J. M.; Cuadros, T. R. M.; Aguilera, J. M. Glass transitions and shrinkage during drying and storage of osmosed apple pieces. *Food Research International***1998**, *31*(3), 191-204.

For Peer Review Only

[80] Krokida, M. K.; Maroulis, Z. B. Effect of drying method on shrinkage and porosity. *Drying technology***1997**, *15*(10), 2441-2458.

[81] Krokida, M. K.; Maroulis, Z. B.; Saravacos, G. D. The effect of the method of drying on the colour of dehydrated products. *International Journal of Food Science & Technology***2001**, *36*(1), 53-59.

[82] Mattea, M.; Urbicain, M. J.; Rotstein, E. Computer model of shrinkage and deformation of cellular tissue during dehydration. *Chemical Engineering Science***1989**, *44*(12), 2853-2859.

[83] Kowalski, S. J.; Mierzwa, D.; Stasiak, M. Ultrasound-assisted convective drying of apples at different process conditions. *Drying Technology***2017**, *35*(8), 939-947.

[84] Tripathy, P. P.; Kumar, S. Neural network approach for food temperature prediction during solar drying. *International Journal of Thermal Sciences***2009**, *48*(7), 1452-1459.

[85] Khawas, P.; Dash, K.K.; Das, A.J..; Deka, S.C. Modeling and optimization of the process parameters in vacuum drying of culinary banana (Musa ABB) slices by application of artificial neural network and genetic algorithm. *Drying Technology***2016**, 34(4), 491-503.

[86] Aghbashlo, M.; Hosseinpour, S..; Mujumdar, A.S. Application of artificial neural networks (ANNs) in drying technology: a comprehensive review. *Drying Technology***2015**, 33(12), 1397-1462.

For Peer Review Only

Fig captions

Fig. 1. Scheme of the ultrasound-assisted fluidized bed dryer. (1. electromotor and fan, 2. air, 3. three electrical pre-heaters, 4. hot air heaters, 5. wind box, 6. k-type thermocouple, 7. piezoelectric transducers, 8. drying chamber, 9. Samples, 10. electrical control unit, 11. temperature controller, 12. inverter, 13. ultrasound generator, 14. digital balance (±0.01g, max 2000g)).

Fig. 2. Ultrasound equipment arrangement. (**A:** drying chamber, **B:** distributor, **C:** ultrasound generator, **D:** ultrasound transducers, **E:** fastening belt and bolts).

Fig. 3. Schematic diagram and photo of the instron and its equipment. (**A:** Schematic diagram of the instron: 1. spherical indenter with radius of curvature 0.838mm, 2. support, 3. corn kernel, 4. load cell, 5. applied force, **B:** probe, **C:** instron, **D:** load-cell).

Fig. 4. Scheme and photo of the cloudy sky chamber. (Scheme of the cloudy sky chamber: 1. halogen lamp, 2. corn sample, 3. dc power switch, 4. range photograph, 5. camera, 6. dome chamber, 7. reflected light).

Fig. 5. Scheme of the proposed interpretative methods

Fig. 6. Selected neural network structure.

Fig. 7. 90° round section.

Fig. 8. The effect of temperature and frequency on final drying time (Duncan test, similar letter shows no significant difference at 5% of probability). The values of error bars correspond to a cumulated total standard error of the mean (error bar = ± total SEM).
*Standard Error of the Mean

Fig. 9. The effect of temperature and power density on final drying time (Duncan test, similar letter shows no significant difference at 5% of probability).The values of error bars correspond to a cumulated total standard error of the mean (error bar = ± total SEM).
*Standard Error of the Mean

Fig. 10. Effect of various frequencies on final drying time of corn at temperature of 40^{o}C and power density of 14.6 kW/m^{3}.

Fig. 11. Effect of power density on final drying time of corn at temperature of 40^{o}C and frequency of 25 kHz.

Fig. 12. The effect of temperature and frequency on ultimate compressive strength (Duncan test, similar letter shows no significant difference at 5% of probability).The values of error bars correspond to a cumulated total standard error of the mean (error bar = ± total SEM).*Standard Error of the Mean

Fig. 13. The effect of temperature and frequency on toughness of corn kernels (Duncan test, similar letter shows no significant difference at 5% of probability).The values of error bars correspond to a cumulated total standard error of the mean (error bar = ± total SEM).*Standard Error of the Mean

Fig. 14. The effect of temperature and frequency on shrinkage (Duncan test, similar letter shows no significant difference at 5 % of probability).The values of error bars correspond to a cumulated total standard error of the mean (error bar = ± total SEM).*Standard Error of the Mean

Fig. 15. The effect of temperature and frequency on RGB color component (Duncan test, similar letter shows no significant difference at 5% of probability).

Fig. 16. The effect of temperature and frequency on $L^{*}a^{*}b^{*}$ color component (Duncan test, similar letter shows no significant difference at 5% of probability)

Fig. 17. Comparison between experimental and predicted values during training, validation and testing of ANN model: drying time, provided by MATLAB R2013a.

For Peer Review Only

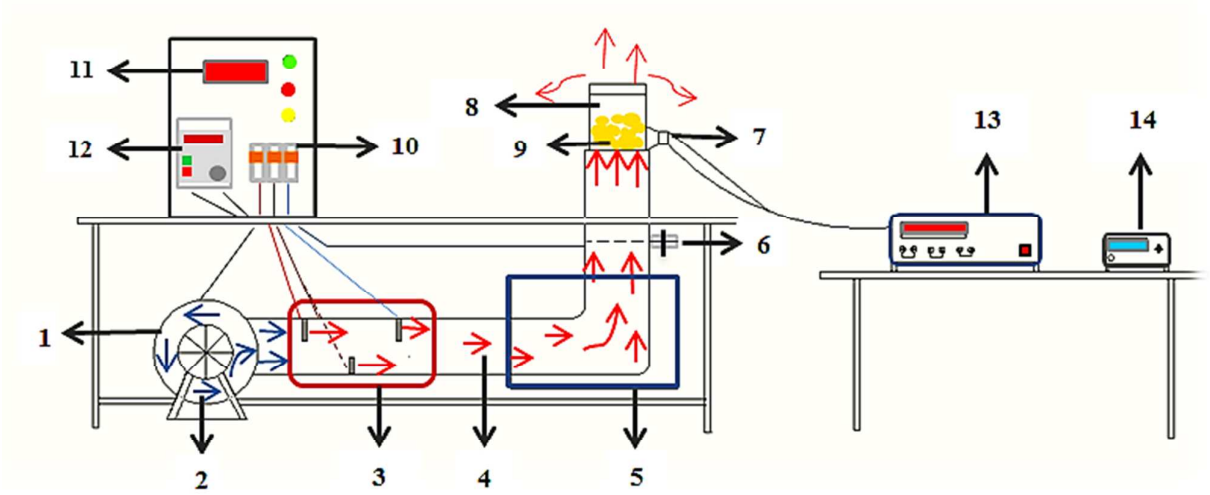

Fig. 1. Scheme of the ultrasound-assisted fluidized bed dryer.
(1. electromotor and fan, 2. air, 3. three electrical pre-heaters, 4. hot air heaters, 5. wind box, 6. k-type thermocouple, 7. piezoelectric transducers, 8. drying chamber, 9. Samples, 10. electrical control unit, 11. temperature controller, 12. inverter, 13. ultrasound generator, 14. digital balance (±0.01g, max 2000g)).

For Peer Review Only

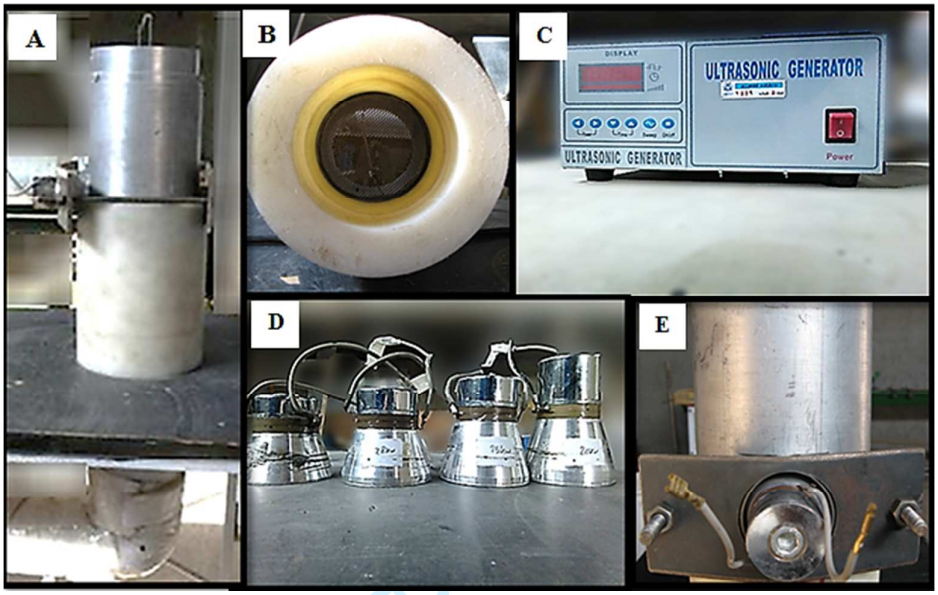

Fig. 2. Ultrasound equipment arrangement.
(**A:** drying chamber, **B:** distributor, **C:** ultrasound generator, **D:** ultrasound transducers, **E:** fastening belt and bolts).

Peer Review Only

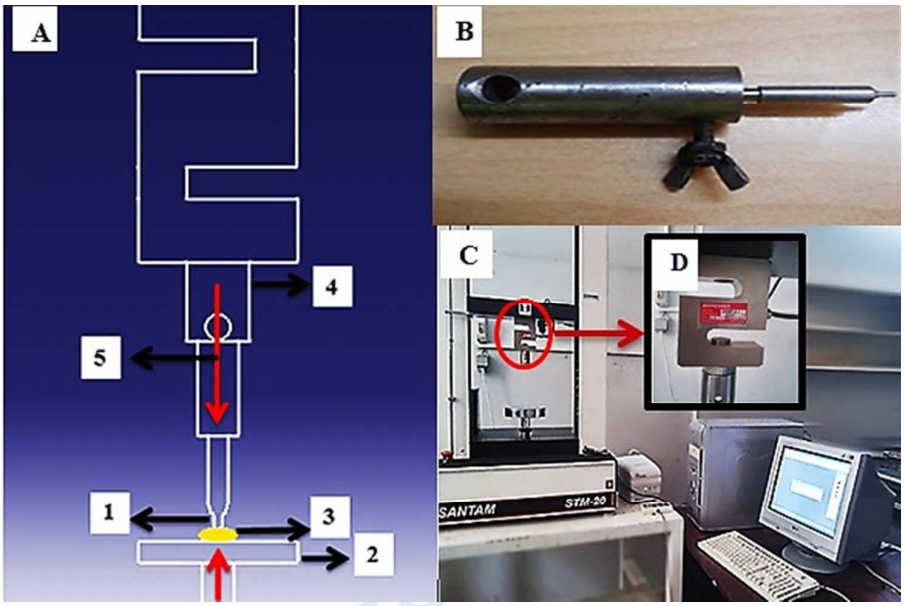

Fig. 3. Schematic diagram and photo of the instron and its equipment.
(**A:** Schematic diagram of the instron: 1. spherical indenter with radius of curvature 0.838mm, 2. support, 3. corn kernel, 4. load cell, 5. applied force, **B:** probe, **C:** instron, **D:** load-cell).

For Peer Review Only

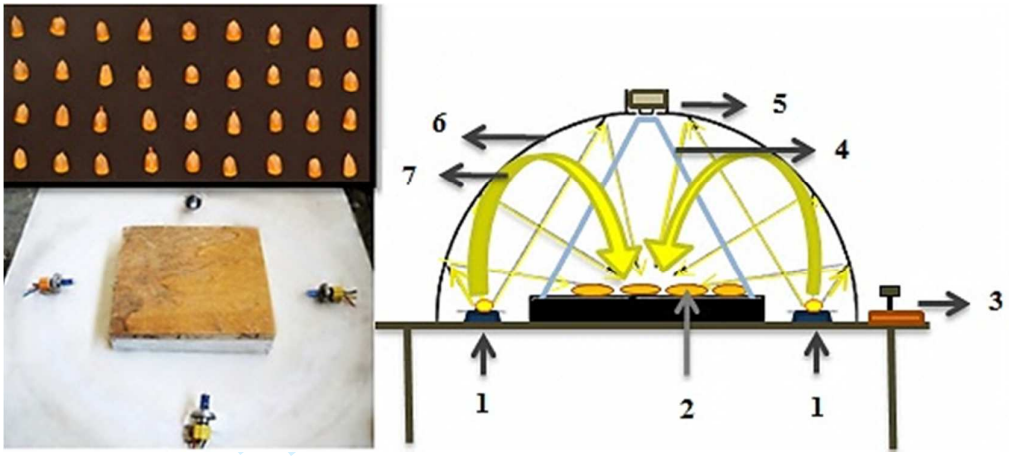

Fig. 4. Scheme and photo of the cloudy sky chamber.
(Scheme of the cloudy sky chamber: 1. halogen lamp, 2. corn sample, 3. dc power switch, 4. range photograph, 5. camera, 6. dome chamber, 7. reflected light).

For Peer Review Only

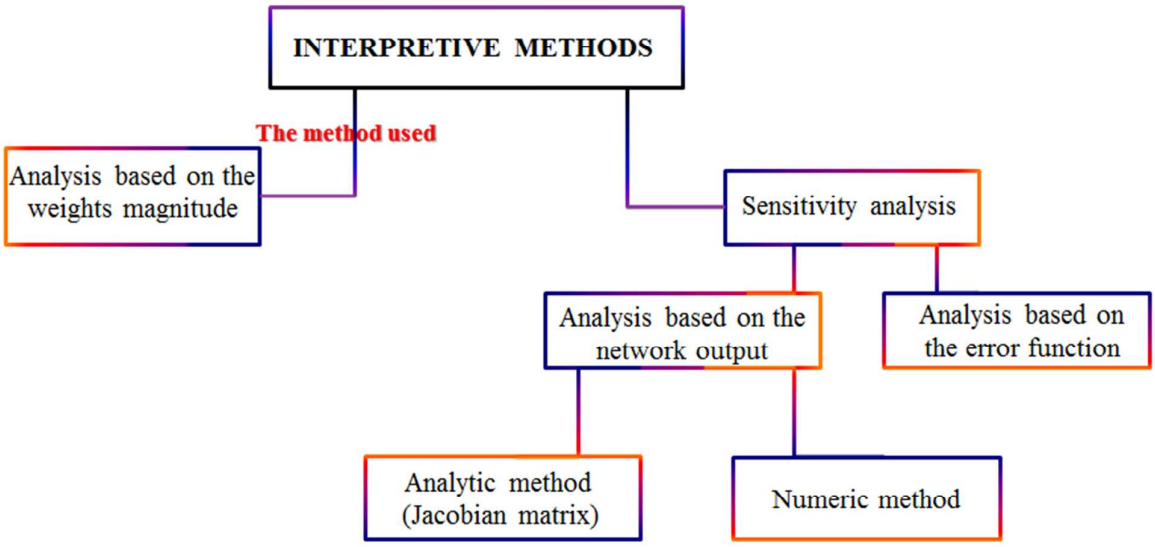

Fig. 5. Scheme of the proposed interpretative methods.

Peer Review Only

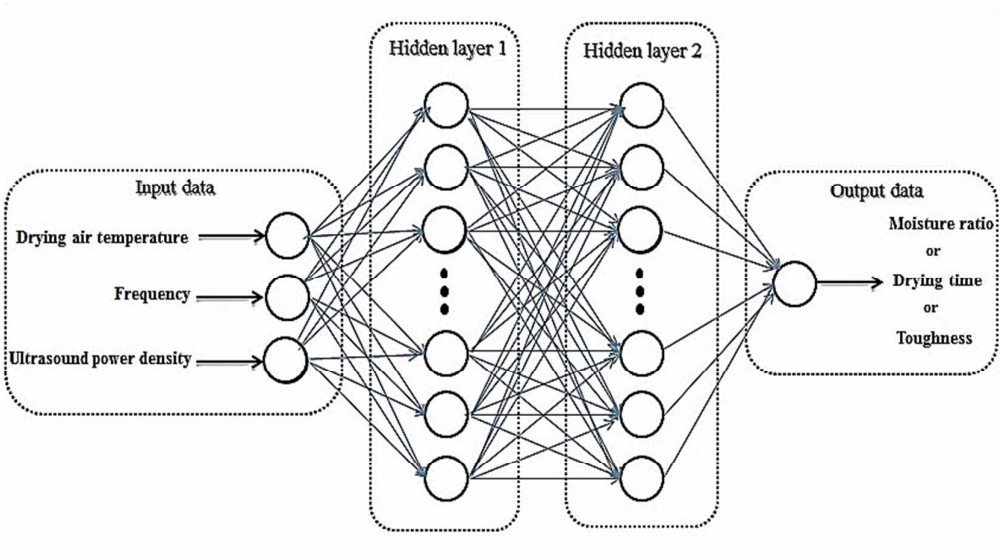

Fig. 6. Selected neural network structure.

Peer Review Only

Fig. 7. 90° round section.

For Peer Review Only

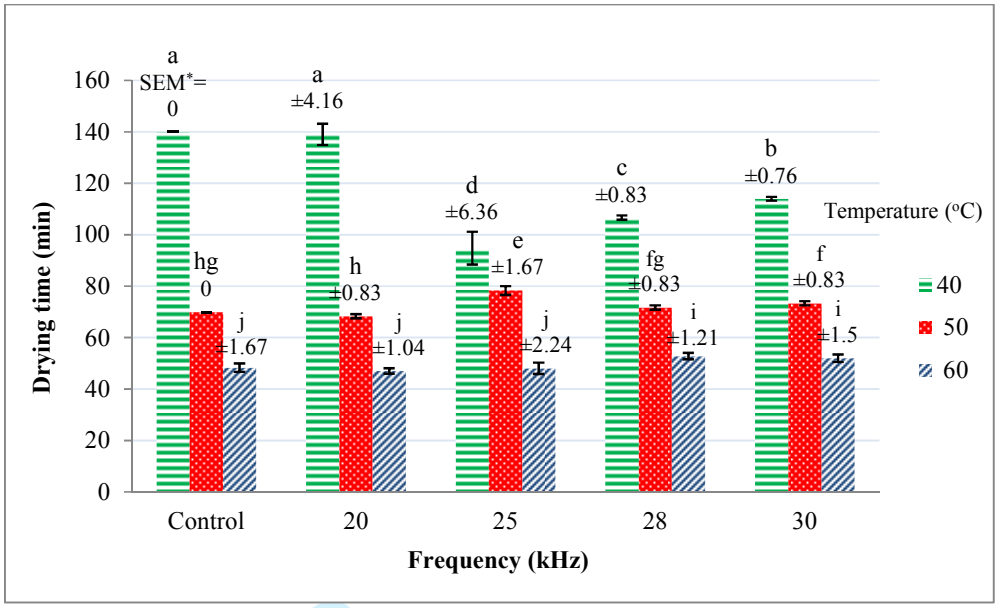

Fig. 8. The effect of temperature and frequency on final drying time (Duncan test, similar letter shows no significant difference at 5% of probability). The values of error bars correspond to a cumulated total standard error of the mean (error bar = ± total SEM).

*Standard Error of the Mean

For Peer Review Only

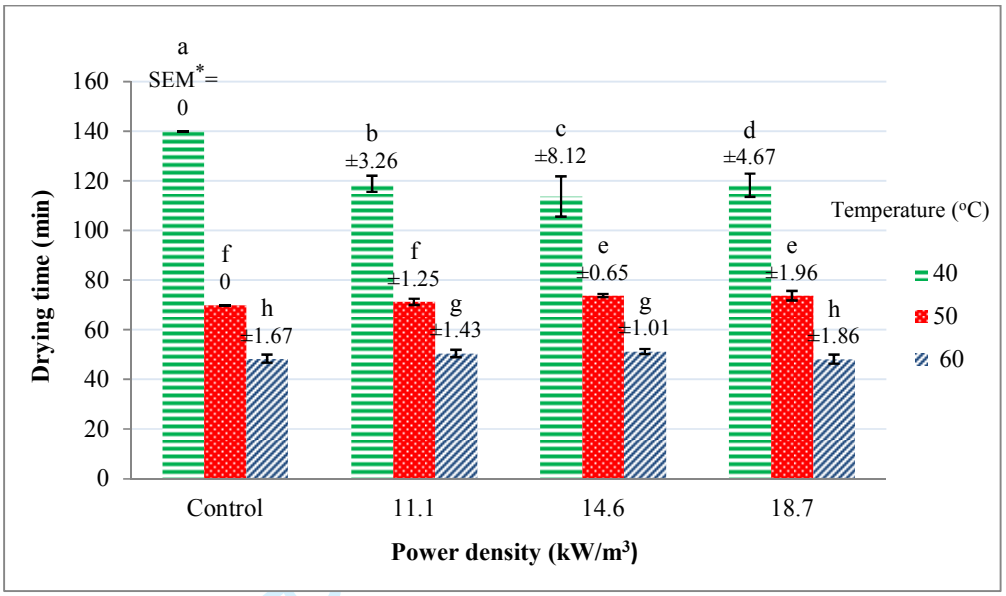

Fig. 9. The effect of temperature and power density on final drying time (Duncan test, similar letter shows no significant difference at 5% of probability).The values of error bars correspond to a cumulated total standard error of the mean (error bar = ± total SEM).

*Standard Error of the Mean

Peer Review Only

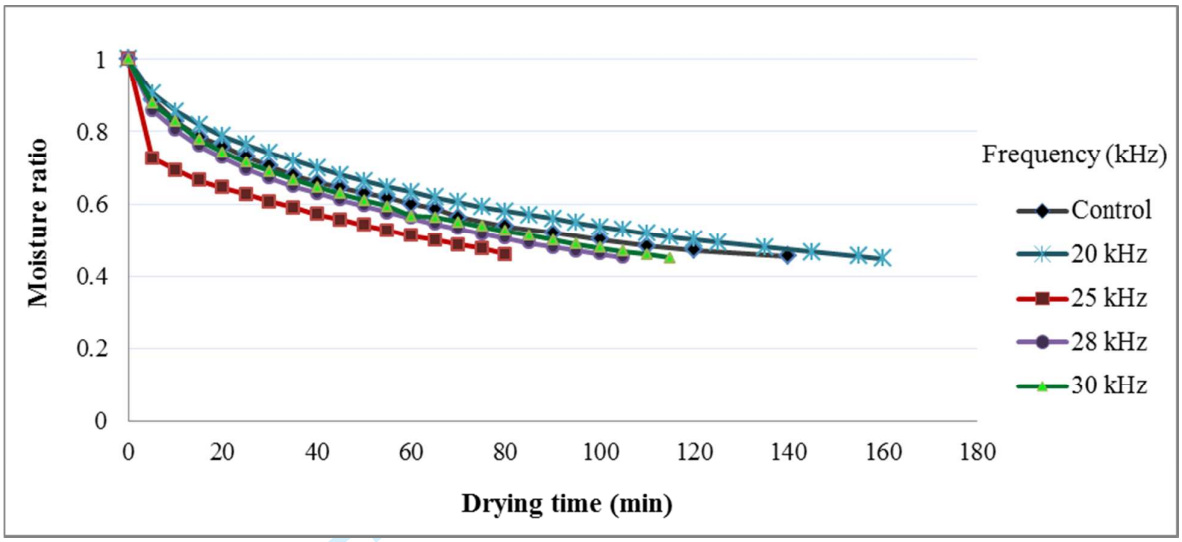

Fig. 10. Effect of various frequencies on final drying time of corn at temperature of 40°C and power density of 14.6 kW/m^3.

For Peer Review Only

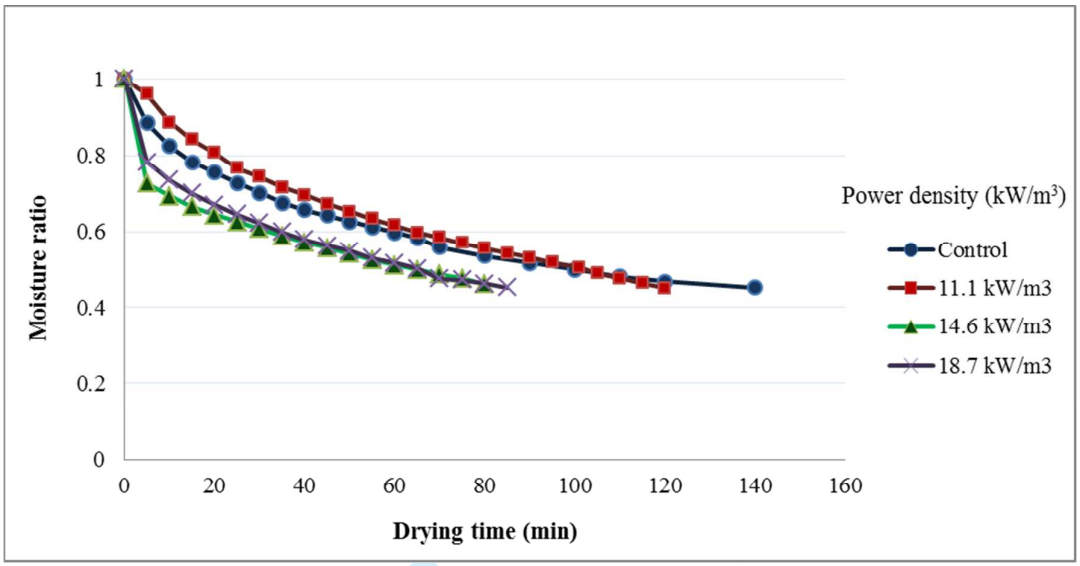

Fig. 11. Effect of power density on final drying time of corn at temperature of 40°C and frequency of 25 kHz.

Peer Review Only

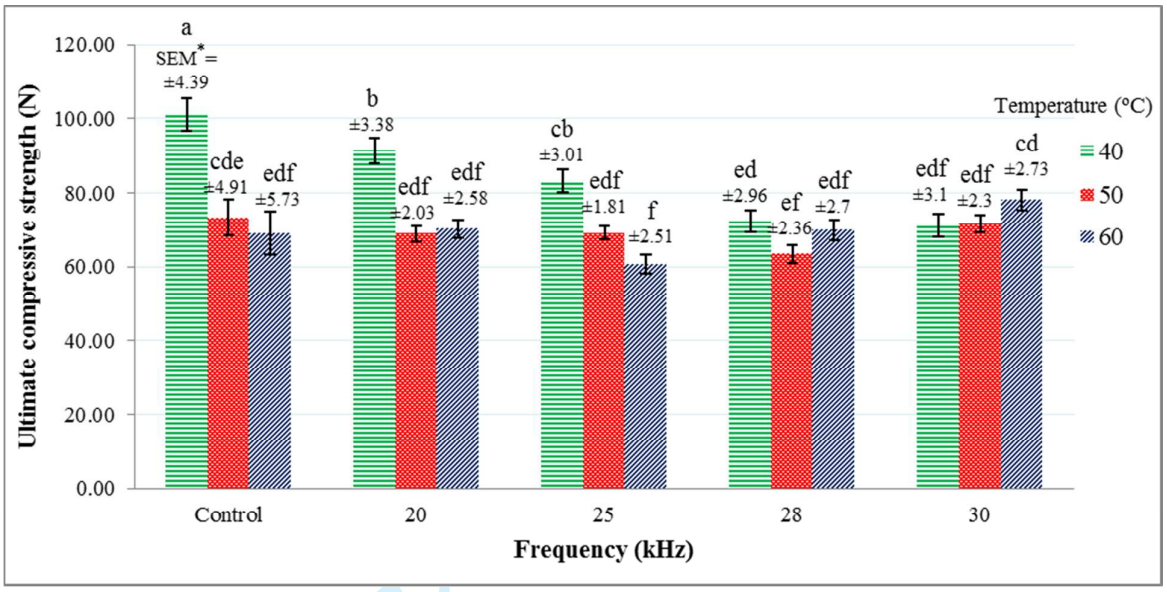

Fig. 12. The effect of temperature and frequency on ultimate compressive strength (Duncan test, similar letter shows no significant difference at 5% of probability).The values of error bars correspond to a cumulated total standard error of the mean (error bar = ± total SEM).

*Standard Error of the Mean

Peer Review Only

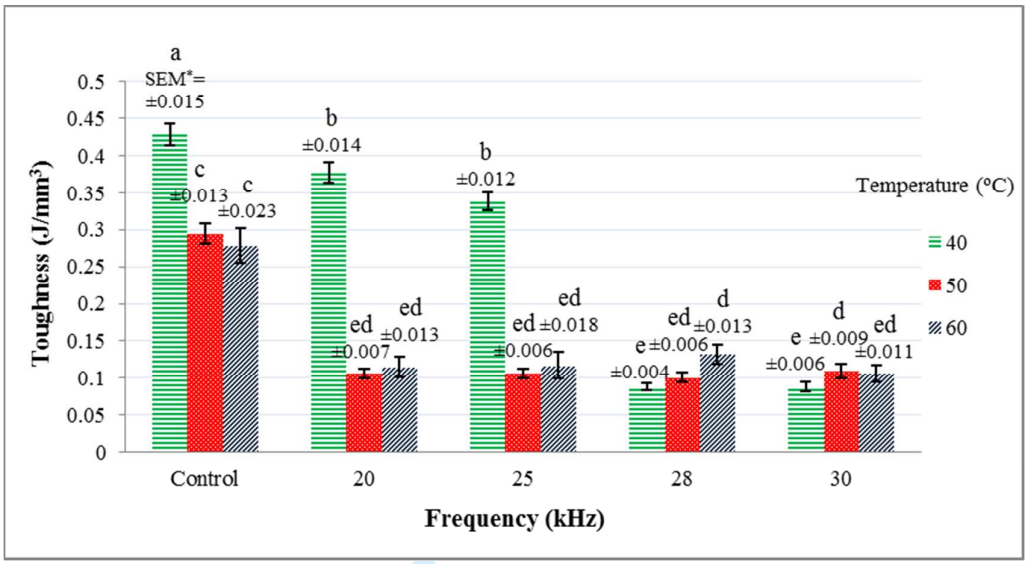

Fig. 13. The effect of temperature and frequency on toughness of corn kernels (Duncan test, similar letter shows no significant difference at 5% of probability).The values of error bars correspond to a cumulated total standard error of the mean (error bar = ± total SEM).

*Standard Error of the Mean

Peer Review Only

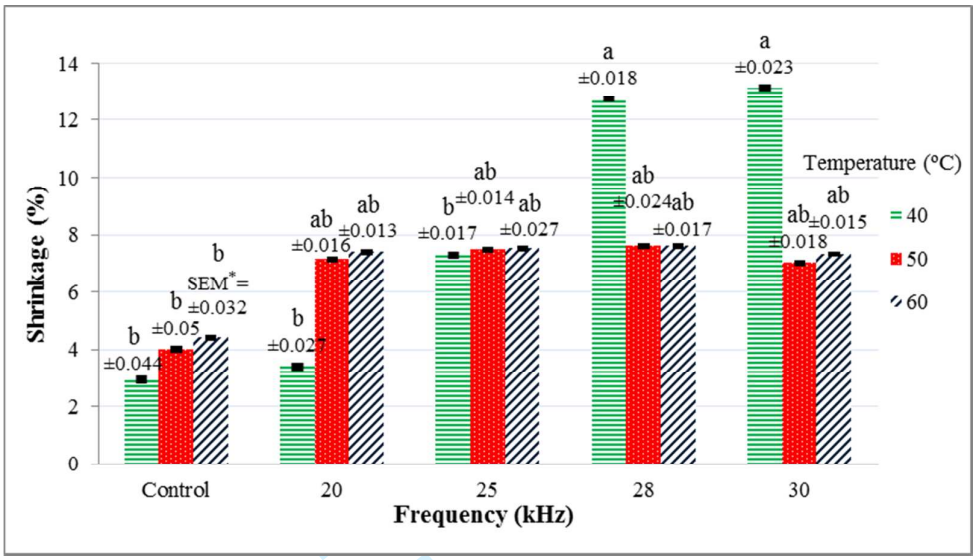

Fig. 14. The effect of temperature and frequency on shrinkage (Duncan test, similar letter shows no significant difference at 5 % of probability).The values of error bars correspond to a cumulated total standard error of the mean (error bar = ± total SEM).

*Standard Error of the Mean

For Peer Review Only

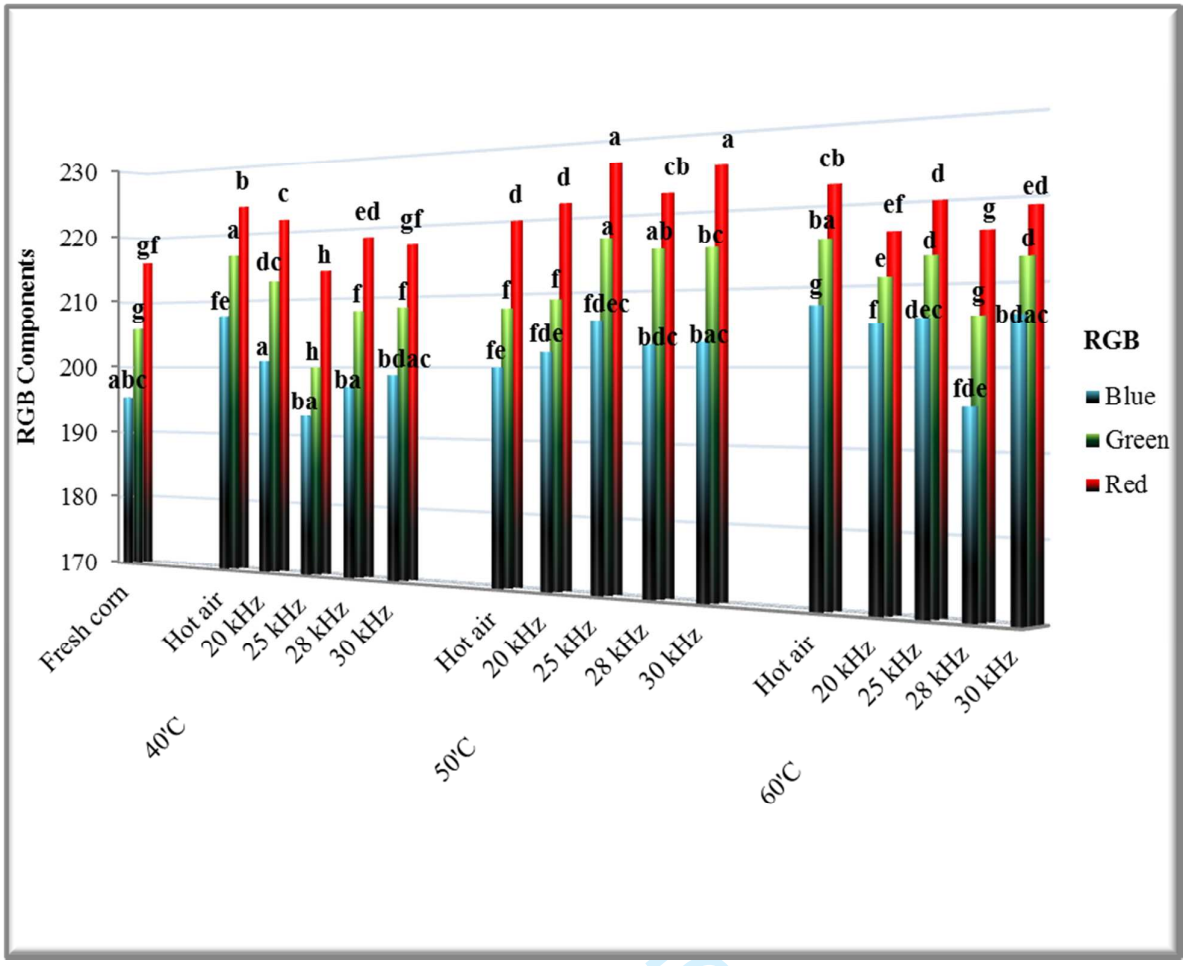

Fig.15. The effect of temperature and frequency on RGB color component (Duncan test, similar letter shows no significant difference at 5% of probability).

For Review Only

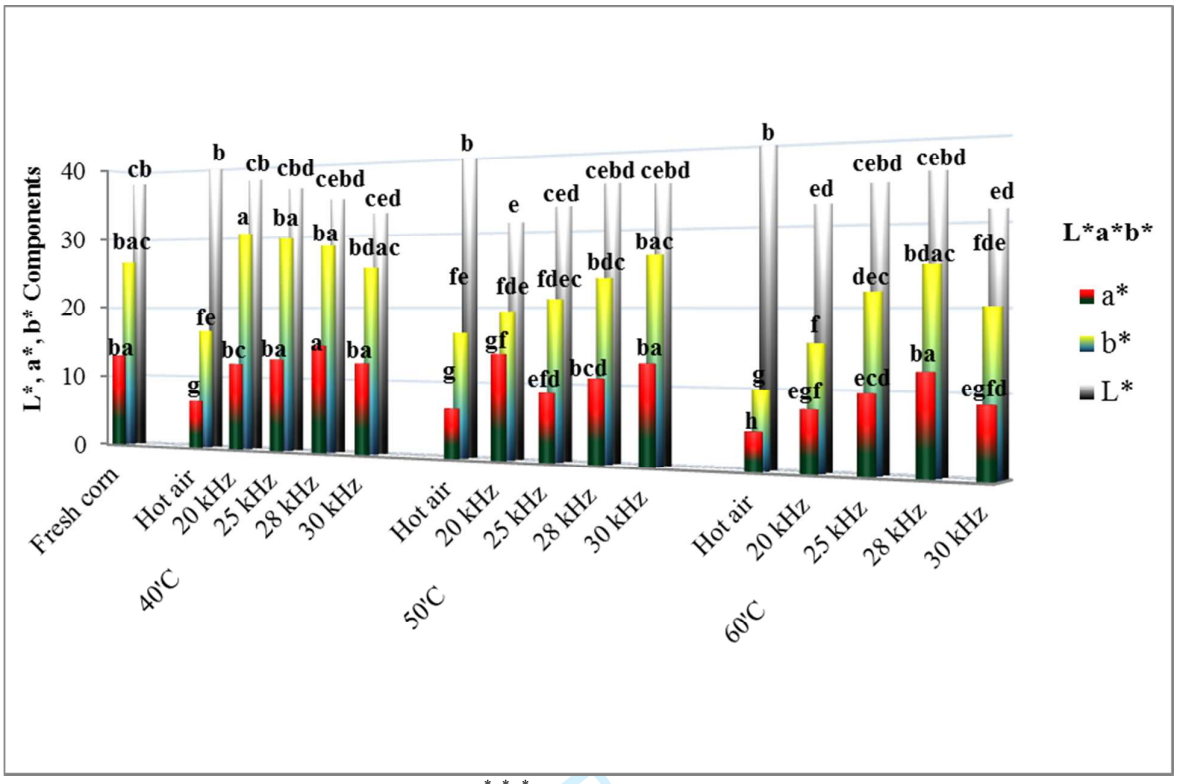

Fig.16. The effect of temperature and frequency on $L^*a^*b^*$ color component (Duncan test, similar letter shows no significant difference at 5% of probability).

Review Only

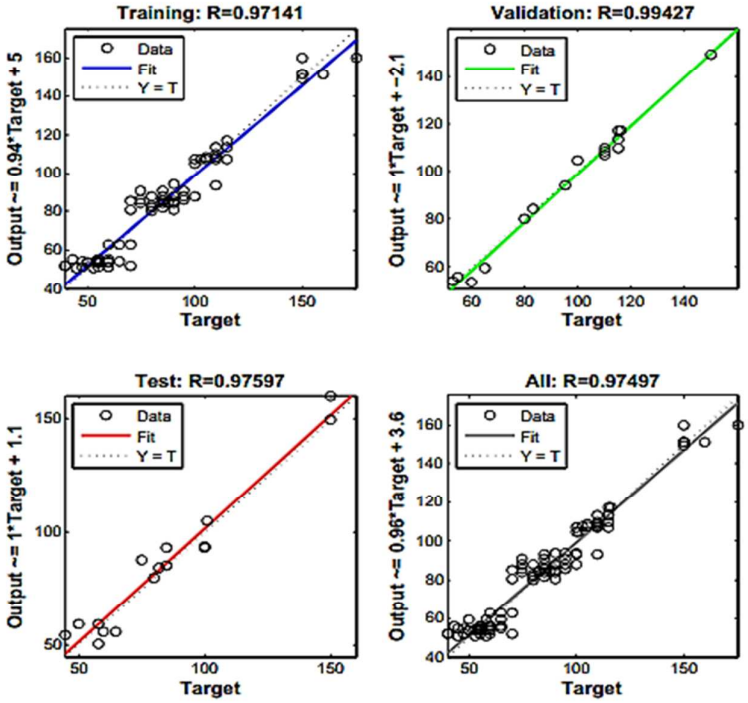

Fig. 17. Comparison between experimental and predicted values during training, validation and testing of ANN model: drying time, provided by MATLAB R2013a.

For Review Only

Table 1. List of transfer functions and back propagation training algorithms used in ANN training

Transfer function	Training algorithms
Logsig (Log sigmoid)	scg (Scaled conjugate gradient back propagation)
Tansig (Hyperbolic tangent sigmoid)	cgp (polak-Ribiere conjugate gradient back propagation)
Poslin (Positive linear)	bfg (BFGS quasi-Newton back propagation)
Satlin (Saturating linear)	lm (Levenberg-Marquardt back propagation)
	rp (Resilient back propagation, Rprop)

For Peer Review Only

Table 2. Final drying time for different treatmentsof cornkernels

Temperature (ºC)	Power density (kW/m^3)	Frequency (kHz) 20	25	28	30	Control
40	11.1	135 ^{c}	120 ^{e}	105 ^{h}	115.33 ^{f}	
	14.6	155 ^{a*}	80 ^{j}	106.67 ^{hg}	113.33 ^{f}	
	18.7	127 ^{d}	84.33 ^{i}	108.33 ^{g}	113.33 ^{f}	
	-	-	-	-	-	140 ^{b}
50	11.1	65 ^{m}	75 ^{k}	70 ^{l}	75 ^{k}	
	14.6	70^{l}	75 ^{k}	75^{k}	75 ^{k}	
	18.7	70^{l}	85^{i}	70 ^{l}	70 ^{l}	
	-	-	-	-	-	70 ^{l}
60	11.1	43 ^{s}	54 ^{on}	50 ^{qp}	55 ^{n}	
	14.6	48^{qr}	50.33 ^{qp}	51.67^{op}	55 ^{n}	
	18.7	50^{qp}	40^{t}	56.67 ^{n}	46 ^{r}	
	-	-	-	-	-	48.33 ^{qr}

* Similar letters indicate no significant difference in the table (Duncan test, at 5 % of probability)

For Peer Review Only

Table 3. Results of the analysis of variance for final drying time of cornkernels

Variables	Degree of freedom	Sum of squares	Mean square error	F
Drying air temperature(T)	2	74788.72	37394.36	16219.2**
Frequency(F)	3	1765.52	588.51	255.26**
Power density(P)	2	247.39	123.69	53.65**
(T)×(P)	4	537.05	134.26	58.23**
(T)×(F)	6	8350.76	1391.79	603.67**
(F)×(P)	6	1658.09	276.35	119.86**
(T)×(F)×(P)	12	2699.46	224.95	97.57**
Error	72	166	2.30	

** Significant at 1% of probability

For Peer Review Only

Table 4. Results of the analysis of variance for ultimate compressive strength of corn kernels

Variables	Degree of freedom	Sum of squares	Mean square error	F
Drying air temperature(T)	2	12040.89	6020.45	17.32^{**}
Frequency(F)	3	5017.23	1672.41	4.81^{**}
Power density(P)	2	481.16	240.58	0.69^{ns}
(T)×(P)	4	1706.24	426.55	1.23^{ns}
(T)×(F)	6	12038.70	2006.45	5.77^{**}
(F)×(P)	6	986.84	164.47	0.47^{ns}
(T)×(F)×(P)	12	1706.40	142.20	0.41^{ns}
Error	565	196446.70	347.69	

** Significant at 1% of probability
^{ns} Non-significant

For Peer Review Only

Table 5. Results of the analysis of variance for toughness of cornkernels

Variables	Degree of freedom	Sum of squares	Mean square error	F
Drying air temperature(T)	2	0.98	0.49	159.92**
Frequency(F)	3	0.56	0.19	60.67**
Power density(P)	2	0.0018	0.00089	0.29ns
(T)×(P)	4	0.022	0.0056	1.83ns
(T)×(F)	6	1.74	0.29	94.77**
(F)×(P)	6	0.025	0.0041	1.35ns
(T)×(F)×(P)	12	0.055	0.0046	1.51ns
Error	399	1.22	0.0031	

** Significant at 1% of probability
ns Non-significant

For Peer Review Only

Table 6. Results of the analysis of variance for shrinkage of cornkernels

Variables	Degree of freedom	Sum of squares	Mean square error	F
Drying air temperature(T)	2	0.0013	0.0006	0.10^{ns}
Frequency(F)	3	0.0416	0.0139	0.10^{ns}
Power density(P)	2	0.0013	0.0006	2.21^{ns}
(T)×(P)	4	0.0135	0.0034	0.54^{ns}
(T)×(F)	6	0.0877	0.0146	0.04^{*}
(F)×(P)	6	0.0099	0.0016	0.95^{ns}
(T)×(F)×(P)	12	0.0518	0.0043	0.76^{ns}
Error	156	0.9804	0.0062	

* Significant at 5% of probability
^{ns}Non-significant

For Peer Review Only

Table 7. The best ANN models for prediction of three outputs

Model output	Topology (number of neurons in each layer)	Transfer function	Number of training cycle	Coefficient of determination (R^2)	Mean square error (MSE)	Mean absolute error (MAE)	Mean relative error (MRE)
Drying Time	3-14-15-1	tansig-logsig	3	0.97	9.14	5.29	0.072
Toughness	3-17-19-1	tansig-tansig	5	0.85	0.002	0.013	0.109
Moisture content	3-10-11-1	tansig-tansig	8	0.80	5.13×10^{-6}	0.007	0.013

For Peer Review Only

Table 8. SEC (MJ/kg) of drying process for different treatments of cornkernels

Temperature (ºC)	Power density (kW/m^3)	Frequency (kHz) 20	25	28	30	Control
	11.1	45.78	39.35	38.37	39.36	
40	14.6	56.15	28.70	38.03	35.77	
	18.7	49.06	30.35	40.98	42.27	
	-	-	-	-	-	42.14
	11.1	26.55	31.38	26.78	32.02	
50	14.6	29.78	33.60	29.89	32.48	
	18.7	34.87	40.51	32.44	32.62	
	-	-	-	-	-	26.21
	11.1	21.10	26.90	24.88	27.43	
60	14.6	25.73	27.25	26.61	28.95	
	18.7	29.42	22.19	30.68	25.77	
	-	-	-	-	-	20.03

For Peer Review Only